

# Ratchet without spatial asymmetry for controlling the motion of magnetic flux quanta using time-asymmetric drives

DAVID COLE<sup>1</sup>, SIMON BENDING<sup>1\*</sup>, SERGEY SAVEL'EV<sup>2,3</sup>, ALEXANDER GRIGORENKO<sup>4</sup>, TSUYOSHI TAMEGAI<sup>5</sup> AND FRANCO NORI<sup>2,6</sup>

<sup>1</sup>Department of Physics, University of Bath, Claverton Down, Bath BA2 7AY, UK

<sup>2</sup>Frontier Research System, The Institute of Physical and Chemical Research (RIKEN), Wako-shi, Saitama 351-0198, Japan

<sup>3</sup>Department of Physics, Loughborough University, Loughborough LE11 3TU, UK

<sup>4</sup>Department of Physics and Astronomy, University of Manchester, Manchester M13 9PL, UK

<sup>5</sup>Department of Applied Physics, The University of Tokyo, 7-3-1 Hongo, Bunkyo-ku, Tokyo 113-8656, Japan

<sup>6</sup>Center for Theoretical Physics, Department of Physics, The University of Michigan, Ann Arbor, Michigan 48109-1040, USA

\*e-mail: pyssb@bath.ac.uk

Published online: 12 March 2006; doi:10.1038/nmat1608

Initially inspired by biological motors, new types of nanodevice have been proposed for controlling the motion of nanoparticles. Structures incorporating spatially asymmetric potential profiles (ratchet substrates) have been realized experimentally to manipulate vortices in superconductors, particles in asymmetric silicon pores, as well as charged particles through artificial pores and arrays of optical tweezers. Using theoretical ideas, we demonstrate experimentally how to guide flux quanta in layered superconductors using a drive that is asymmetric in time instead of being asymmetric in space. By varying the time-asymmetry of the drive, we are able experimentally to increase or decrease the density of magnetic flux at the centre of superconducting samples that have no spatial ratchet substrate. This is the first ratchet without a ratchet potential. The experimental results can be well described by numerical simulations considering the dragging effect of two types of vortices penetrating layered superconductors in tilted magnetic fields.

**B**iological motors<sup>1,2</sup> are anisotropic devices that, when driven by non-equilibrium fluctuations, bias the motion of particles. These motors have inspired novel solid-state devices (see, for example, refs 1–23) for controlling the motion of nanoparticles, electrons and colloidal particles, as well as for particle separation<sup>6</sup>, smoothing atomic surfaces<sup>7</sup>, and manipulation of superconducting magnetic flux quanta<sup>8–11</sup>. Some of these devices have been realized experimentally to manipulate vortices<sup>12–18</sup>, particles in asymmetric silicon pores<sup>5</sup>, as well as charged particles through artificial pores<sup>19,20</sup> and arrays of optical tweezers<sup>21–23</sup>. The controlled transport of magnetic flux quanta in superconductors<sup>8–18</sup> would allow the realization of magnetic flux pumps, diodes and lenses to ‘sculpt’ desired magnetic profiles within a sample. There is also a huge interest in exploiting the control of flux motion in flux qubits for quantum computation<sup>24</sup>, as well as finding ways to remove vortices from active (for example, superconducting quantum interferometer devices—SQUIDs) and passive (for example, filters) superconducting devices because they lead to large amounts of unwanted noise.

Several novel approaches to the problem of vortex motion control in superconductors, using asymmetric nanofabricated pinning potentials, have been proposed<sup>8–11</sup> and realized<sup>12–18</sup> by a number of groups. These new devices can be tuneable (for example, the polarity of the magnetic flux rectifier<sup>13</sup> can be changed by varying the applied magnetic field and the amplitude of the alternating current drive). However, once the devices are fabricated, there is no way to change the asymmetric ‘ratchet potential’ that governs their transport properties. This limits the degree of control of the motion of flux quanta, and it would be very desirable to have a much more malleable and adjustable device concept.

Inspired by on-going experiments on the transport of K and Rb ions in ion channels<sup>25</sup>, particles of different sizes in asymmetric

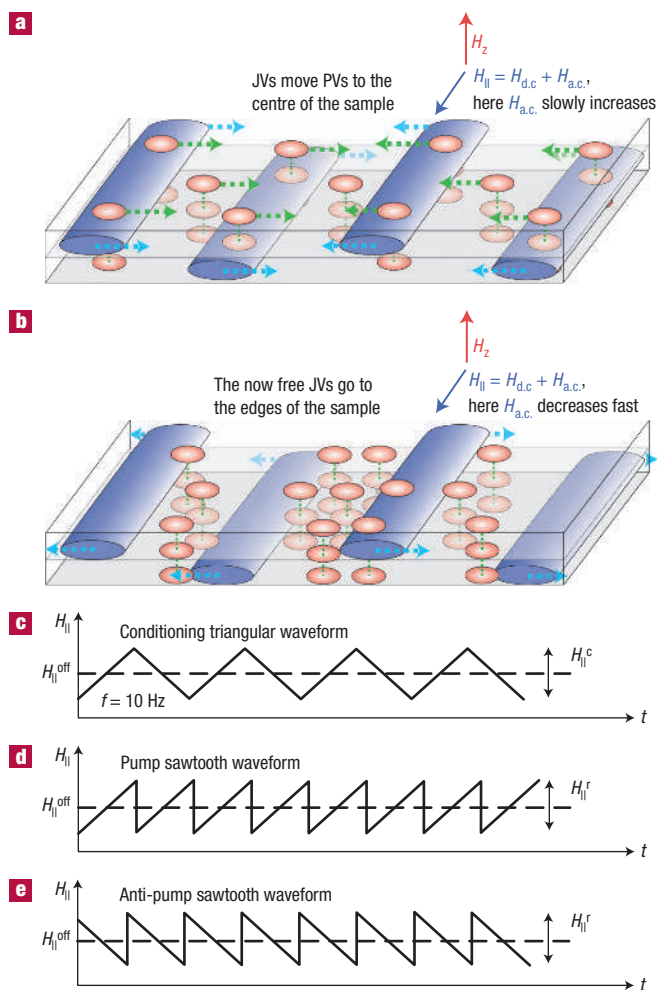


**Figure 1** Introduction to the operation of the ratchet device. **a,b**, Schematic diagrams of the vortex lens operation: **a**, the slowly driven JVs, shown by the green horizontal cylinders, drag vertical PV stacks, shown in red, towards the sample's centre. **b**, JVs moving quickly towards the sample's edges leave behind PVs. **c–e**, The shape of the pulses used in the experiments and simulations for the a.c.-driven lensing mode: **c**, conditioning triangular waveform (symmetric) to equilibrate PVs, **d**, pump and **e**, antipump asymmetric sawtooth waveforms. Here the superscript off refers to offset, c to conditioning and r to ratchet.

silicon pores<sup>5</sup> and interpenetrating lattices of different vortices<sup>26–32</sup>, a technique to control tiny particles in binary mixtures has been proposed<sup>33,34</sup>. Remarkably, this particle motion control can be achieved using periodic time-asymmetric drives in samples with no ratchet substrate. When one of the components of the binary mixture is driven, the moving particles drag along the other non-driven component, interacting with it. A time-asymmetric a.c.-drive (as opposed to a time-symmetric a.c.-drive and spatially asymmetric substrate in 'conventional' ratchet devices) produces a net d.c. motion of both components of the binary mixture, which can be tuned by means of the time-dependence and time-asymmetry of the drive (see for example, movies of ref. 35). The device acts like a ratchet, but it has no ratchet potential energy. We present the first experimental demonstration of the tuneable control of the motion of magnetic flux quanta without spatially asymmetric substrates. Our approach can be readily extended to many other types of binary mixture (for example, colloids<sup>21–23</sup>).

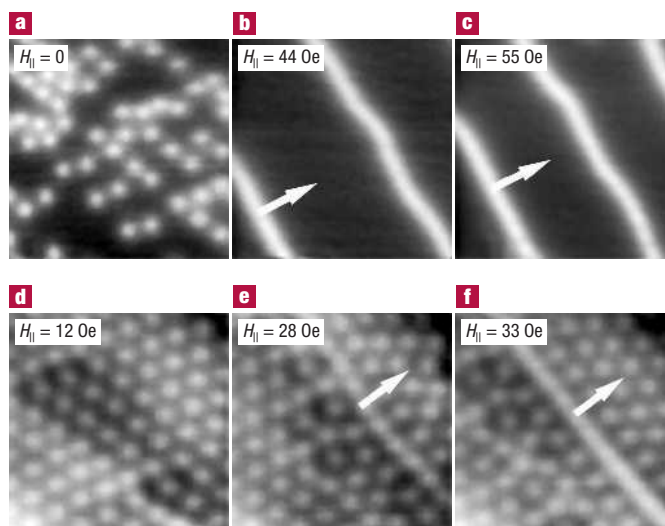


**Figure 2** Experimental scanning Hall probe images of dragging/brushing of PVs by JV stacks. **a–c**, Trapping of PVs (white spots) onto chains by JVs (not visible), and subsequent dragging of PVs by moving JVs as  $H_{\parallel}$  is systematically increased from 0 to 55 Oe. The sample was initially field cooled to  $T = 81$  K in  $H_z \sim 1.5$  Oe (scan sizes  $\sim 27 \mu\text{m} \times 27 \mu\text{m}$ ). **d–f**, 'Brushing' of PVs by moving JVs at high PV densities as  $H_{\parallel}$  is varied between 0 and 33 Oe.  $T = 77$  K,  $H_z = 10$  Oe (scan sizes  $\sim 13 \mu\text{m} \times 13 \mu\text{m}$ ). The arrows indicate the direction of JV motion.

It has been recognized<sup>33</sup> that this new ratchet concept can be implemented experimentally in layered superconductors such as  $\text{Bi}_2\text{Sr}_2\text{CaCu}_2\text{O}_{8+\delta}$  (Bi2212). In this system, direct visualization<sup>26–29</sup>, as well as magnetic<sup>30,31</sup> and transport<sup>32</sup> measurements, clearly show that a magnetic field, tilted away from the high-symmetry crystalline  $c$ -axis, penetrates the sample as two perpendicular vortex arrays, known as 'crossing' vortex lattices<sup>36–38</sup>. One vortex sublattice consists of stacks of pancake vortices (PVs) aligned along the  $c$  axis, whereas the other is formed by Josephson vortices (JVs) confined between  $\text{CuO}_2$  layers (Fig. 1a,b). It was predicted<sup>37,38</sup> that JVs attract PVs, and this PV–JV interaction has been experimentally observed<sup>26–29</sup> through the formation of PV chains on top of JVs. Sensitive a.c. measurements<sup>39</sup> have also verified the existence of dragging interactions between JVs and PVs. JVs are usually very weakly pinned and can be easily driven by changing either the in-plane magnetic field,  $H_{\parallel}$ , or applying an electrical current,  $J_z$ , flowing along the  $c$ -axis. Time-asymmetrically driven JVs can drag along PVs, resulting in a net motion of the PVs. It was shown<sup>33</sup> that this common JV–PV motion could be used to develop vortex-pumps, vortex-diodes and vortex-lenses. The vortex lens operation is illustrated schematically in Fig. 1a,b.

#### D.C.-DRIVEN LENSING

The simplest possible operation mode consists of slowly increasing the in-plane field,  $H_{\parallel}$ , from 0 to  $H_{\parallel}^{\text{max}}$  for a fixed value of the out-of-plane magnetic field,  $H_z$ . The increasing in-plane field slowly drives JVs from the edges to the middle of the sample. In turn, JVs drag PVs along with them towards the sample's centre. As a result, PVs accumulate in the middle of this magnetic 'lens'. Figure 2a–c shows a set of experimental images of the dragging of PVs by JVs at a low out-of-plane field,  $H_z \sim 1.5$  Oe. At such low PV densities, all of the PVs are first trapped on JV stacks and then dragged towards the sample's centre. Figure 2d–f illustrates PV 'brushing' for a higher

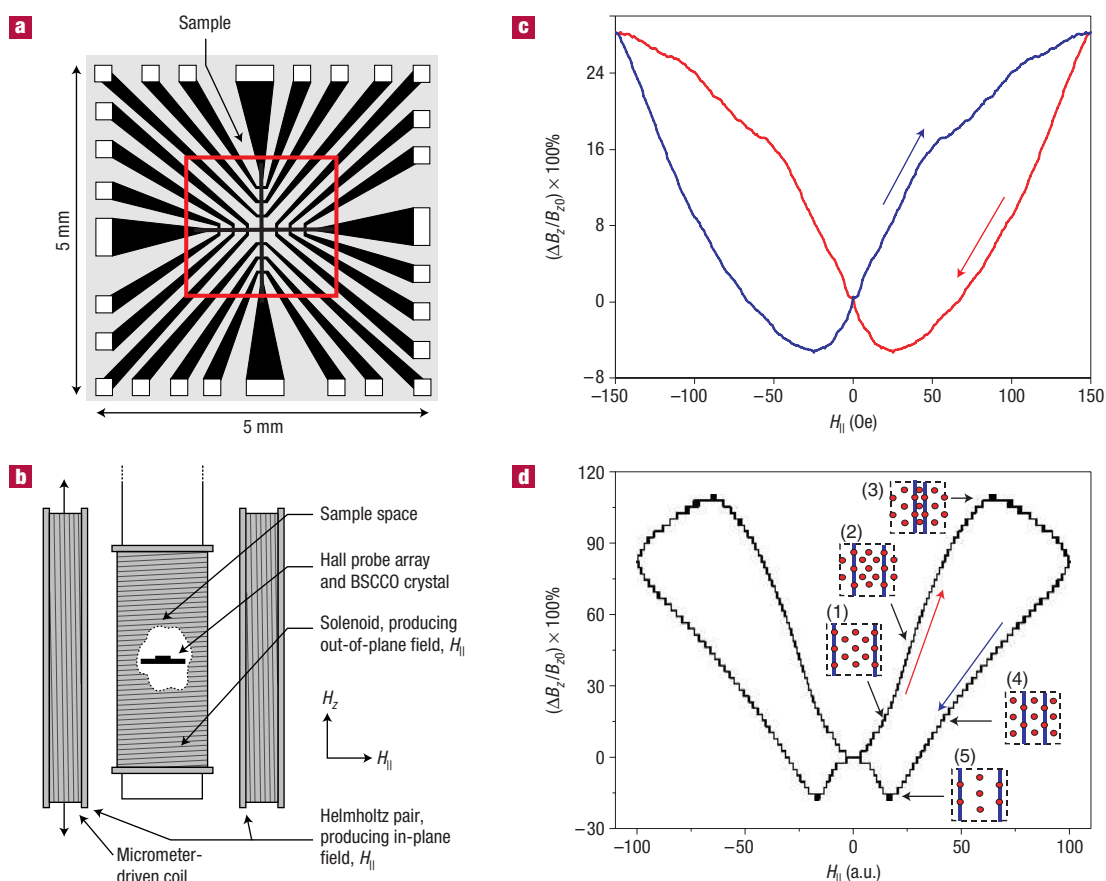


**Figure 3 Results of d.c. lensing.** **a**, Schematic diagram of the Hall probe array beneath the sample. The grey box indicates the position of the Bi2212 crystal. **b**, The experimental setup to separately control the in-plane,  $H_{||}$ , and the out-of-plane,  $H_z$ , magnetic fields. **c**, A characteristic ‘butterfly’ loop for the lensing efficiency in d.c.-driven lensing mode at  $T = 77$  K and  $H_z = 5.3$  Oe.  $B_{z0} = B_z(H_{||} = 0)$ . **d**, Results of simulations of d.c.-driven lensing. (1)–(5) schematically show vortex distributions at different points on the  $\Delta B_z(H_{||})$  butterfly loop for an idealized situation where we consider transport of PVs by only two JV rows. (1) Two blue JV rows start moving towards the sample’s centre, compressing 13 PVs. (2) All 13 PVs remain trapped on or between JVs, resulting in an increase of PV density at the sample’s centre. Notice that four new PVs have now entered at the sample edges. (3) Additional movement of the JVs towards the centre results in further compression of the PVs. However, PV–PV repulsion now causes PVs to spill out across JVs and only 7 of the original 13 PVs remain trapped. (4) When  $H_{||}$  decreases, JVs move towards the sample edges, pushing the PVs located close to the surface out of the sample; hence only the remaining 7 PVs trapped between the JVs contribute to the central PV density. (5) At the position of the overshoot for decreasing  $H_{||}$ , only 7 PVs (instead of the initial 13 PVs) remain in the sample, and anti-lensing is observed. Further reduction of  $H_{||}$  results in all JVs leaving the sample, deficit PVs can re-enter and the original PV density is restored.

out-of-plane field,  $H_z \sim 10$  Oe, which is closer to the situation when the strongest lensing effects are observed. At these high PV densities, JV traps become saturated and free PVs exist between them. Moving JVs now ‘brush’ free PVs in their direction of motion, giving rise to a higher density ahead of them and a lower density behind them (see also the movies of ref. 35).

### A.C.-DRIVEN LENSING

When a superposition of d.c. and time-asymmetric a.c. (compare Fig. 1d,e) in-plane magnetic fields is applied,  $H_{||}(t) = H_{||}^{\text{d.c.}} + H_{||}^{\text{a.c.}}(t)$ , the JVs are asymmetrically pushed in and pulled out of the sample. If the a.c. component of  $H_{||}$  increases slowly, the PV stacks remain trapped on JVs, and both move together towards the centre of the lens (Fig. 1a). If, on the way back,  $H_{||}^{\text{a.c.}}$  decreases rapidly (Fig. 1d, pump sawtooth waveform), the JVs leave the PVs behind them (Fig. 1b). Asymmetrically cycling  $H_{||}^{\text{a.c.}}$  causes either pumping (focusing) or antipumping (defocusing) of PVs at the centre of the lens<sup>35</sup>. An important advantage of such an a.c.-driven vortex lens is

that switching between ‘convex’ and ‘concave’ PV ‘magnetic lenses’ can be easily achieved by changing the asymmetry of the applied a.c. field, for example, by using a time-reversed sawtooth waveform (for example Fig. 1e).

### EXPERIMENTAL RESULTS FOR D.C. AND ASYMMETRIC A.C. LENSING MODES

Our vortex lensing experiments were carried out on an as-grown Bi2212 superconducting single crystal (transition temperature  $T_c \cong 91$  K, size  $\sim 1$  mm  $\times$  0.75 mm  $\times$  50  $\mu\text{m}$ ). The changes in magnetic induction, arising from PV lensing/anti-lensing, were detected using one centrally placed (with respect to the Bi2212 crystal) element of a 25  $\mu\text{m}$  wire-width micro-Hall probe array, patterned in a GaAs/AlGaAs 2D electron gas (Fig. 3a). The in-plane,  $H_{||}$ , and out-of-plane,  $H_z$ , magnetic field components were varied independently using a Helmholtz coil pair, precisely aligned to the  $a$ – $b$  crystallographic planes of the crystal, and a solenoid, respectively (Fig. 3b).

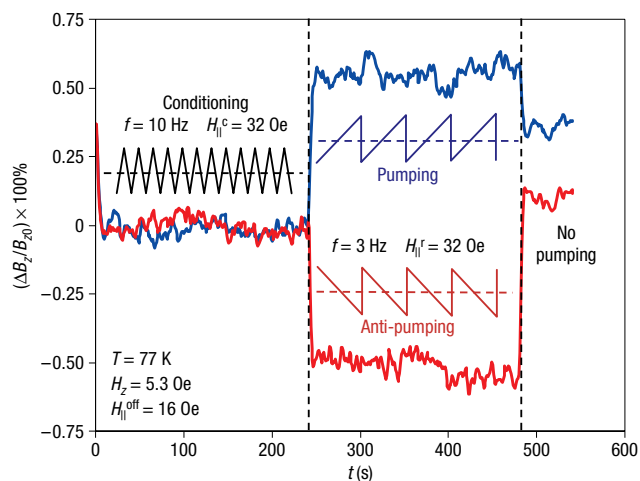


**Figure 4** Time dependence of the a.c.-driven ratchet device. The curves show the measured percentage change of the magnetic induction (PV density) at the sample's centre, when applying an initial 'conditioning' signal followed by pumping/antipumping time-asymmetric drives. The conditioned PV density increases (decreases) during several cycles of the pumping (antipumping) drive and then saturates. As soon as the drive is switched off, the PV density starts to relax from the non-equilibrium pumping (antipumping) state towards an equilibrium state.

We carried out measurements for both d.c.-driven modes and asymmetric a.c.-driven modes of vortex lens operation. Initially, a fixed PV density was established in our crystal by field cooling from above  $T_c$  in a known value of the out-of-plane field,  $H_z$ . In the d.c.-mode, the in-plane magnetic field,  $H_{||}$ , was then slowly ( $1.7 \text{ Oe s}^{-1}$ ) cycled a few times until a steady-state loop was obtained. During each cycle,  $H_{||}$  was ramped up to a maximum of 150 Oe, then down to a minimum of  $-150 \text{ Oe}$  and back to zero, while the sensor Hall voltage was monitored to measure the magnetic induction at the centre of the sample. Figure 3c shows lensing data at 77 K, for an out-of-plane magnetic field,  $H_z = 5.3 \text{ Oe}$ , when the lensing efficiency (defined by the overall percentage change of the PV density at the sample's centre,  $\kappa = \{[\max(B_z^{\text{centre}}) - \min(B_z^{\text{centre}})]/B_z^{\text{centre}}(H_{||} = 0)\} \times 100\%$ ) reaches a maximum of about 37% for this temperature. Here,  $B_z^{\text{centre}}$  is the out-of-plane magnetic induction at the centre of the crystal. The d.c.-driven lensing mode exhibits a butterfly shape comprising: (1) a fast increase of PV density at the centre when  $H_{||}$  increases from zero, followed by a weaker (saturation-like) dependence of  $B_z^{\text{centre}}(H_{||})$ ; (2) a rapid reduction of  $B_z^{\text{centre}}(H_{||})$  when  $H_{||}$  decreases from its maximum value, followed by a remarkable anti-lensing (an overshoot in the reduction of PV density) effect,  $B_z^{\text{centre}}(H_{||} > 0) < B_z^{\text{centre}}(H_{||} = 0)$ . We note that this 'overshoot' effect is not seen for low out-of-plane magnetic fields ( $H_z < 2 \text{ Oe}$ ) when all PVs are trapped at JVs. At higher values of  $H_z$ , JV traps become saturated and free PVs exist between chains (the so-called mixed chains plus lattice state). The overshoot effect is clearly correlated with the presence of these free PVs, and has been systematically observed for  $H_z > 2 \text{ Oe}$  at Hall elements in different locations over a wide temperature range.

In order to realize the asymmetric a.c.-driven mode for the vortex lens, the following steps were carried out. (1) The sample was cooled in fixed  $H_z$  at  $H_{||} = 0$ ; (2) a d.c. offset value of the in-plane field,  $H_{||}^{\text{off}}$ , was applied; (3) a 'conditioning' triangular wave (see Fig. 1c) was run for 4 min to equilibrate the PV system; (4) a time-asymmetric a.c. drive, with an average value of zero

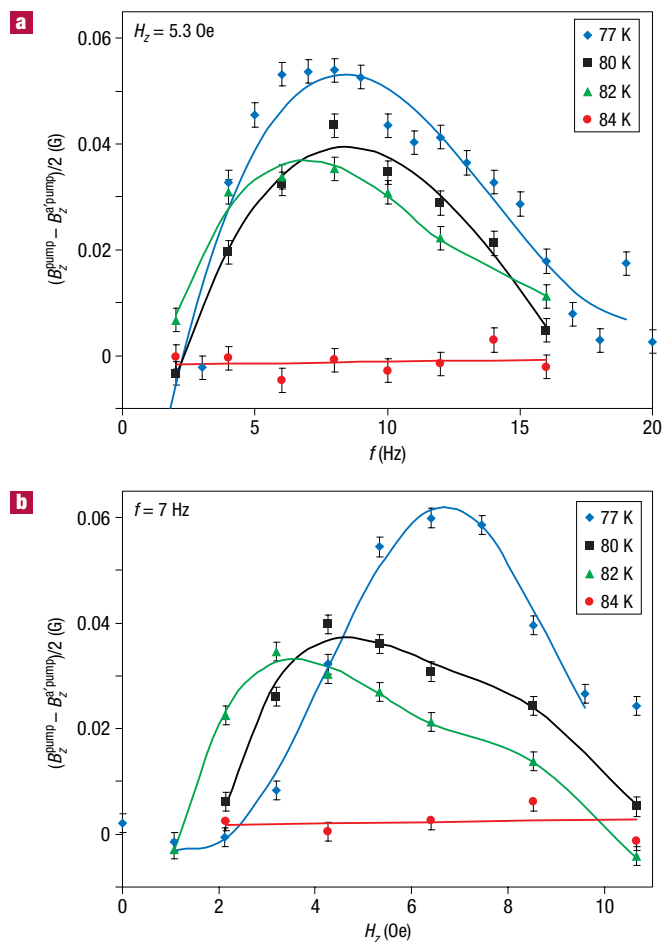


**Figure 5** Investigations of lensing efficiency. The dependence of the lensing amplitude on **a**, the frequency of the ratchet signal ( $H_{||}^{\text{off}} = 80 \text{ Oe}$ ,  $H_{||}^r(1 \text{ Hz}) = 80 \text{ Oe}$ ,  $H_z = 5.3 \text{ Oe}$ ) and **b**, the applied out-of-plane field,  $H_z$  ( $H_{||}^{\text{off}} = 80 \text{ Oe}$ ,  $H_{||}^r = 80 \text{ Oe}$ ,  $f = 7 \text{ Hz}$ ), at different temperatures. Both dependencies exhibit pronounced maxima allowing the lensing efficiency to a desirable value. Superscript pump (a/pump) refers to pumping (antipumping). The error bars predominantly reflect the average fluctuation amplitude in the measured magnetic induction during pumping/anti-pumping of the vortex system (see Fig. 4).

(Fig. 1d,e) was switched on for 4 min. The magnetic induction,  $B_z^{\text{centre}}$ , was then monitored in real time starting from step (3) at a centrally located Hall element. The data from one such measurement is presented in Fig. 4. The initial rapid transients (see Fig. 4), as the conditioning waveform is switched on at  $t = 0$ , are due to equilibration of the PV system from non-equilibrium states generated in previous ratchet experiments. As soon as the asymmetric pumping (antipumping) signal is switched on, the density of PVs ( $B_z^{\text{centre}}/\Phi_0$ , where  $\Phi_0$  is the quantum of magnetic flux) starts to increase (decrease) in the centre of the vortex lens with respect to the PV density produced after application of only the conditioning signal ( $B_z^{\text{centre}}(\text{conditioning})/\Phi_0$ ). After several cycles of the asymmetric sawtooth in-plane magnetic field, the PV density reaches a steady-state value for both pumping ( $B_z^{\text{centre}}(\text{pumping})/\Phi_0$ ) and antipumping ( $B_z^{\text{centre}}(\text{antipumping})/\Phi_0$ ) regimes, respectively (Fig. 4). We stress that these steady pumping (antipumping) states are essentially non-equilibrium ones, because they relax towards close states as soon as the time-asymmetric drive is switched off (Fig. 4). Hence, we experimentally show how to

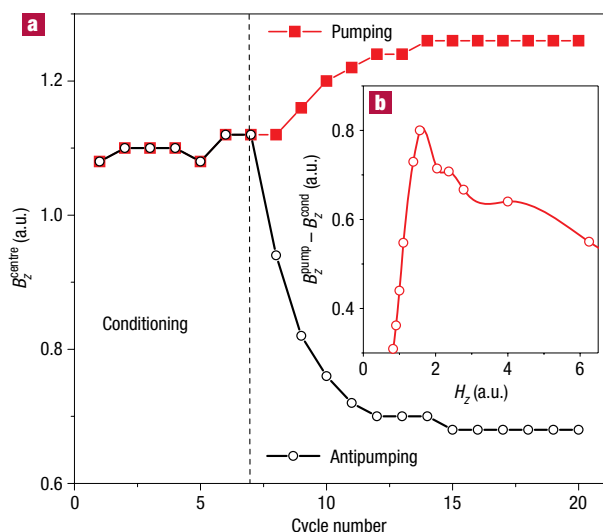


**Figure 6** The simulated asymmetrically a.c.-driven vortex lens. **a**, The dependence of the out-of-plane magnetic induction at the centre of the sample,  $B_z^{\text{centre}}$ , on the cycle number when conditioning and pumping/antipumping drives are applied. **b**, Pumping amplitude versus the out-of-plane magnetic field,  $H_z$ . In both experiments and simulations the pumping efficiency exhibits pronounced maxima as a function of  $H_z$ .

control the out-of-equilibrium vortex transport. Such control of the motion of vortices (or other tiny particles) is the ultimate goal of ratchet devices<sup>1–23</sup>.

The two main advantages of the transport control developed here over previous proposals (for example, refs 8–18) are (1) the possibility to guide particles with no tailored spatial asymmetry and (2) the tuning of the motion of tiny particles by simply changing the time-dependence of the externally applied drive. The first feature allows us to avoid expensive and cumbersome nanofabrication processing. The second property becomes very important if we want to frequently change the transport properties of a device, something which is generally much more complicated or even impossible in standard ratchet devices.

#### TUNEABILITY OF THE VORTEX LENS USING AN ASYMMETRIC A.C. DRIVE

A simple switch from the pumping to the time-reversed anti-pumping sawtooth  $H_{\parallel}$  waveform results in a change from PV focusing to defocusing at the centre of the sample. As was predicted theoretically<sup>33,34</sup>, the focusing efficiency can also easily be controlled by changing either the frequency of the drive,  $f$ , (Fig. 5a) or the PV density, by means of the out-of-plane magnetic field component,  $H_z$  (Fig. 5b). Note that both of these two ‘knobs’ (tuning the frequency of the applied drive or the particle density) are common to other realizations of these ratchets, including mixtures of ions in ion channels<sup>25</sup> and particles of different sizes in silicon pores<sup>5</sup>. Moreover, varying the temperature changes the interaction between PVs and JVs, which also influences the lensing effect and can provide additional degrees of controllability.

The frequency dependence (Fig. 5a) of the non-equilibrium pumping (antipumping) can be qualitatively understood using general arguments. For low frequencies, the effect should be small because the repetition rate is low, and the PV density has enough time to reach its equilibrium value during both ‘slow’ and ‘fast’ changes of the time-asymmetric drive. PVs adiabatically move back and forth without accumulation in the sample’s centre. For very

high frequencies, the vortex system cannot follow the drive, even during relatively ‘slow’ changes of the in-plane field,  $H_{\parallel}$ . Thus, the PVs just ignore the fast magnetic-field oscillations, and again settle in an equilibrium state. Assuming an analytical behaviour of the lensing efficiency for low and high frequencies, it should be proportional to  $f$  and  $1/f$ , when  $f \rightarrow 0$  and  $f \rightarrow \infty$ , respectively. In addition, the leakage of PVs parallel to JVs could suppress the ratchet effect at low frequencies. Suppression at high frequency depends on the ratio of (1) the strength of the interaction between PVs and JVs divided by (2) the PV viscosity, which slows down the transport of PVs by JVs. The interaction between JVs and PVs depends nonlinearly on the JV velocity in a complex way. Hence this ratio depends on several parameters, and cannot be easily estimated. The maximum lensing efficiency occurs when the PVs adiabatically follow the slow changes of  $H_{\parallel}$  but cannot follow the fast changes. The maximum of the lensing efficiency as  $H_z$  is varied (Fig. 5b), can also be understood noting that the interaction of JVs and PVs, and thus the dragging effect, becomes negligible with respect to PV–PV repulsive interactions at high PV densities (high  $H_z$ ). For low  $H_z$ , the decreasing PV density, and the domination of PV pinning over the JV–PV interaction, diminish the lensing effect. Thus, there should be an optimal out-of-plane field,  $H_z$ , for the operation of the vortex lens.

#### NUMERICAL SIMULATIONS

The minimum model to simulate the observed lensing effect describes the overdamped dynamics of JV and PV rows within a set of coupled equations of motion:  $\gamma\eta_j(dx_i^j/dt)/a^j = f_i^j + f_i^{jH} + f_i^{jP}$  and  $\eta_p(dx_k^p/dt)/a^p = f_k^{pp} + f_k^{pH} + f_k^{pJ}$ , where  $x_i^j$  and  $x_k^p$  are the positions of JV and PV rows with  $a^j/\gamma$  and  $a^p$  the distances between JVs and PVs in a row, respectively. Here,  $\gamma$  is the anisotropy parameter, and the JV and PV viscosities are  $\eta_j$  and  $\eta_p$ . The viscous forces (all forces per unit area) slowing down the vortex motion are balanced by: (1) the repulsive force  $f^{jJ}$  between vertical JV rows (including images of rows with respect to the sample surface); (2) the interaction  $f^{jH}$  of JV rows with Meissner currents generated by the externally applied time-dependent magnetic field,  $H_{\parallel}(t)$ ; (3) the repulsion  $f^{pp}$  between rows of PV stacks (including images); (4) the interaction  $f^{pH}$  of PV rows with the  $c$ -axis magnetic field,  $H_z$ ; and (5) the attractive forces  $f^{jP}$  and  $f^{pJ}$  between rows of JVs and PVs. Within our 1D model, PVs do not move parallel to JVs. Thus, this model describes weak (with respect to the JV–PV interaction) bulk pinning plus surface pinning, prohibiting the escape of PVs along the JVs.

#### COMPARISON THEORY–EXPERIMENT

Molecular dynamics simulations were carried out for both d.c. and a.c. lensing modes. Following experiments for the d.c.-driven mode,  $H_{\parallel}$  increases from zero to  $H_{\parallel}^{\text{max}}$  and then decreases back to zero over the same period of time, after which the same half-cycle is repeated for negative fields. The simulated ‘butterfly’ loop for the PV density at the centre of the sample shows the same features that were observed in experiments (compare Fig. 3c and d) and can be easily interpreted: (1)  $B_z^{\text{centre}}$  first increases with  $H_{\parallel}$  on the rising branch of the loop as JVs move towards the centre of the sample, dragging PVs with them (Fig. 2a–f). This is consistent with theoretical predictions<sup>33</sup>; (2) at a certain in-plane field,  $B_z^{\text{centre}}$  saturates and even starts to decrease. The PV density at the centre is now large enough that the enhanced PV–PV repulsion starts to oppose any additional lensing. (In the experiments, the decrease of  $B_z^{\text{centre}}$  was not clearly observed on the rising branch of the loop because of limits on the maximum possible in-plane field.) At this point JVs start cutting freely through PV stacks; (3) once the

in-plane sweep direction is reversed, the additional PV–PV ‘pressure’ now acts in the same direction as the JV dragging force, and a rapid decompression of the PV system takes place. At large values of  $H_z$ , this even causes the system to overshoot and reduce the PV density below its starting value. This gives rise to a remarkable anti-lensing effect,  $B_z^{\text{centre}}(H_{\parallel} > 0) < B_z^{\text{centre}}(H_{\parallel} = 0)$ , which is seen in both experiments and simulations within a certain interval  $0 < H_{\parallel} < H_{\parallel}^*$  of the in-plane field. A more detailed study of the d.c. lensing mode, including the distribution of PVs in the sample, shows excellent qualitative agreement between the experimental data and simulations.

In order to better understand the time-asymmetric a.c.-driven effect, we simulate the experimental sequence of steps: (1) first applying an offset in-plane field, (2) followed by a conditioning (symmetric triangular) drive (Fig. 1c) and finally (3) an asymmetric sawtooth a.c. drive (Fig. 1d,e). The result of these simulations is an increase of  $B_z^{\text{centre}}$  for the pump sawtooth and a decrease for the antipump sawtooth, as illustrated in Fig. 6a, and in excellent agreement with experiments and theoretical predictions<sup>33</sup>. In the focusing mode,  $(B_z^{\text{pump}} - B_z^{\text{cond}})$  exhibits a pronounced maximum as a function of  $H_z$  (Fig. 6b) and frequency (not shown), also in agreement with experimental findings.

## METHODS

### EXPERIMENTAL

Experiments were carried out on an as-grown Bi2212 single crystal prepared by the travelling floating zone technique<sup>40</sup>. The 13-element Hall array (Fig. 3a) was based on the intersection of 25- $\mu\text{m}$ -wide ‘wires’ patterned in a GaAs/AlGaAs heterostructure<sup>41</sup>. All of the measurements described here were made on an element that was centrally positioned under the Bi2212 crystal. This was driven by a 45  $\mu\text{A}$  300 Hz a.c. current and the Hall voltage was detected with a lock-in amplifier.

The in-plane field,  $H_{\parallel}$ , must be precisely aligned with the Bi2212  $a$ – $b$  planes. For an applied magnetic field at an angle  $\theta$  to these (for  $\gamma < 1.95\lambda(T)/s$ , where  $\gamma$  is the anisotropy parameter and  $s$  the  $\text{CuO}_2$  layer separation) a sharp ‘lock-in’ feature is predicted<sup>42</sup> for  $\theta \leq s/\lambda(T)$ , corresponding to complete screening of  $H_z$ . This is clearly observed in our Hall data, and exploited to align a pair of Helmholtz coils that generate in-plane fields. One of these coils is fixed at the height of the sample, and the other is free to move up or down on a micrometer-driven stage. The locus of values of in-plane lock-in field as a function of height of this moving coil is used to infer the perfect alignment position within  $\pm 0.006^\circ$  of the  $a$ – $b$  planes.

The d.c.-mode lensing data were captured by slowly ramping the in-plane field,  $H_{\parallel}$ , (ramp rate = 1.7  $\text{G s}^{-1}$ ) up to a maximum of 150 Oe, then down to a minimum of  $-150$  Oe and back to zero. The first trace obtained in this way shows a pronounced asymmetry because it starts from the virgin field-cooled state. Figure 3c in this paper corresponds to ‘work hardened’ data, after several full field cycles had been completed, which show a high degree of symmetry.

In a.c.-driven measurements, the slope of the rapidly changing part of the sawtooth field was governed by the inductive response of the Helmholtz coil pair ( $dH_{\parallel}/dt$  (fast)  $\sim \pm H_{\parallel}^c R/L$ , where  $R = 8 \Omega$  and  $L = 24$  mH are the resistance and inductance of the coil pair, and  $r$  refers to ratchet). The slope of the slowly changing part increased approximately linearly with frequency,  $f$ , as  $dH_{\parallel}/dt$  (slow)  $\sim \pm H_{\parallel}^c f$ . The  $H_{\parallel}$ -drive amplitude in Fig. 5a was set at  $f = 1$  Hz, and decreased slightly with increasing frequency ( $\sim 20\%$  from 1 to 20 Hz) due to the finite characteristic response time of the coil pair ( $L/R \sim 3$  ms).

A protocol was developed to equilibrate the PV system after each ratchet experiment. Avraham *et al.*<sup>43</sup> showed that the PV system in Bi2212 single crystals is effectively equilibrated by ‘dithering’ with an 80 Oe, 1 kHz a.c. in-plane field. We find that a symmetric (in time) triangular wave ( $H_{\parallel}^c = 32$  Oe, where  $c$  refers to conditioning,  $f = 10$  Hz) is most effective in our field and temperature regime.

The lensing amplitude in Fig. 5 drops to virtually zero above  $T = 84$  K, which is well below  $T_c \cong 91$  K in a regime where the JV–PV interaction strength is only very weakly temperature dependent<sup>37</sup>. We note that efficient lensing actually requires finite pinning (bulk pinning will drop rapidly at high temperatures) as JV stacks only represent one-dimensional traps for PVs, which must be prevented from escaping focus regions laterally parallel to JVs.

### MOLECULAR DYNAMICS MODEL

The interaction between vortex rows decays exponentially for both PVs and JVs:  $f_j^{\text{J}} \tau a^j / (\gamma D \eta_j) = (a^p \beta / a^j) \sum_k \text{sgn}[x_k^j - x_j^j] \exp[-|x_k^j - x_j^j|/\lambda_c]$ ,  $f_k^{\text{PV}} \tau a^p / D \eta_p = \sum_j \text{sgn}[x_k^p - x_j^p] \exp[-|x_k^p - x_j^p|/\lambda_{ab}]$ , where the interaction lengths are the in-plane  $\lambda_{ab}$  and  $c$ -axis  $\lambda_c$  penetration lengths, and  $\beta = \eta_p / \gamma \eta_j$  is the relative viscosity. We normalize all of the distances by the half-width of the sample  $D$ , and all time scales by  $\tau = 16\pi\lambda_{ab}^2 a^p \eta_p D / \Phi_0^2$ . The distances between PV and JV rows are related to the  $c$ -axis  $H_z$  and in-plane  $H_{\parallel}$  magnetic field components as  $a^p \approx (\Phi_0/H_z)^{1/2}$  and  $a^j \approx (\gamma\Phi_0/H_{\parallel})^{1/2}$ . The interaction with the Meissner current decays exponentially on the scales  $\lambda_c$  and  $\lambda_{ab}$  from the surface ( $x = \pm 1$ ) of the sample, for JVs and PVs, respectively. The corresponding forces can be modelled<sup>44</sup> as  $f_j^{\text{JH}} \tau a^j / \gamma D \eta_j = -(2\lambda_c a^p \beta / (a^j)^2) \sinh[x_k^j / \lambda_c] / \cosh[D/\lambda_c]$  and  $f_k^{\text{PVH}} \tau a^p / D \eta_p = -(2\lambda_{ab} / a^p) \sinh[x_k^p / \lambda_{ab}] / \cosh[D/\lambda_{ab}]$ . The simplest way to estimate the JV–PV attraction is to introduce an ‘effective’ potential<sup>33</sup>. This results in the following forces  $f_j^{\text{J}} \tau a^j / \gamma D \eta_j = [(\lambda_{ab})^2 \beta \beta_1 / (a^j)^2] \sum_k \text{sgn}[x_k^j - x_j^j] \exp[-4\pi|x_k^j - x_j^j|/a^j]$ , and  $f_k^{\text{PV}} \tau a^p / D \eta_p = [(\lambda_{ab})^2 a^p \beta_1 / (a^p)^2] \sum_j \text{sgn}[x_k^p - x_j^p] \exp[-4\pi|x_k^p - x_j^p|/a^p]$ , where the parameter  $\beta_1 \approx 16\pi^2 / \ln[1 + [(\lambda_c/a^j)^2 + 1]/[(\lambda_{ab}/a^p)^2 + 1]]$  is related to the tilt elasticity of PV stacks. Our experiments usually involve several thousand PV rows, which are hard to simulate, even using the proposed simple model. To avoid this problem we have generally simulated about one hundred PV rows and used appropriately rescaled model parameters:  $\beta = 2$ ,  $\beta_1 = 0.2$ ,  $\lambda_{ab} = 0.006$ ,  $\lambda_c = 0.1$  and the duration of the fast changes of the in-plane field was 100 times shorter than that of the slow changes. The excellent qualitative agreement between the experimental data and simulations justifies all of the approximations used.

Received 14 October 2005; accepted 24 January 2006; published 12 March 2006.

### References

- Hänggi, P., Marchesoni, F. & Nori, F. Brownian motors. *Ann. Phys. (Leipzig)* **14**, 51–70 (2005).
- Hänggi, P. & Marchesoni, F. Introduction: 100 years of Brownian motion. *Chaos* **15**, 026101 (2005).
- Linke, H. *et al.* Experimental tunneling ratchets. *Science* **286**, 2314–2317 (1999).
- Linke, H. (ed.) Ratchets and Brownian motors: Basics, experiments and applications. *Appl. Phys. A 75* (special issue), 167 (2002).
- Matthias, S. & Muller, F. Asymmetric pores in a silicon membrane acting as massively parallel Brownian ratchets. *Nature* **424**, 53–57 (2003).
- Roussellet, J., Salome, L., Ajdari, A. & Prost, J. Directional motion of Brownian particles induced by a periodic asymmetric potential. *Nature* **370**, 446–448 (1994).
- Derenyi, I., Lee, C. & Barabási, A. L. Ratchet effect in surface electromigration: Smoothing surfaces by an ac field. *Phys. Rev. Lett.* **80**, 1473–1476 (1998).
- Wambaugh, J. F. *et al.* Superconducting fluxon pumps and lenses. *Phys. Rev. Lett.* **83**, 5106–5109 (1999).
- Olson, C. J. *et al.* Collective interaction-driven ratchet for transporting flux quanta. *Phys. Rev. Lett.* **87**, 177002 (2001).
- Zhu, B. Y. *et al.* Controlling the motion of magnetic flux quanta. *Phys. Rev. Lett.* **92**, 180602 (2004).
- Lee, C.-S. *et al.* Reducing vortex density in superconductors using the ‘ratchet effect’. *Nature* **400**, 337–340 (1999).
- Kwok, W. K. *et al.* Modification of vortex behavior through heavy ion lithography. *Physica C* **382**, 137–141 (2002).
- Villegas, J. E. *et al.* A superconducting reversible rectifier that controls the motion of magnetic flux quanta. *Science* **302**, 1188–1191 (2003).
- Van de Vondel, J. *et al.* Vortex-rectification effects in films with periodic asymmetric pinning. *Phys. Rev. Lett.* **94**, 057003 (2005).
- Togawa, Y. *et al.* Direct observation of rectified motion of vortices in a niobium superconductor. *Phys. Rev. Lett.* **95**, 087002 (2005).
- Wördenweber, R., Dymashevski, P. & Misko, V. R. Guidance of vortices and the vortex ratchet effect in high- $T_c$  superconducting thin films obtained by arrangement of antidots. *Phys. Rev. B* **69**, 184504 (2004).
- Majer, J. B., Peguiron, J., Grifoni, M., Tusveld, M. & Mooij, J. E. Quantum ratchet effect for vortices. *Phys. Rev. Lett.* **90**, 056802 (2003).
- Shalom, D. E. & Pastoriza, H. Vortex motion rectification in Josephson junction arrays with a ratchet potential. *Phys. Rev. Lett.* **94**, 177001 (2005).
- Siwly, Z. & Fulinski, A. Fabrication of a synthetic nanopore ion pump. *Phys. Rev. Lett.* **89**, 198103 (2002).
- Marquet, C. *et al.* Rectified motion of colloids in asymmetrically structured channels. *Phys. Rev. Lett.* **88**, 168301 (2002).
- Grier, D. G. A revolution in optical manipulation. *Nature* **424**, 810–816 (2003).
- Gopinathan, A. & Grier, D. G. Statistically locked-in transport through periodic potential landscapes. *Phys. Rev. Lett.* **92**, 130602 (2004).
- Lee, S., Ladavac, K., Polin, M. & Grier, D. G. Observation of flux reversal in a symmetric optical thermal ratchet. *Phys. Rev. Lett.* **94**, 110601 (2005).
- You, J. Q. & Nori, F. Superconducting circuits and quantum information. *Phys. Today* **58**, 42–47 (2005).
- Morais-Cabral, J. H. *et al.* Energetic optimization of ion conduction rate by the K+ selectivity filter. *Nature* **414**, 37–42 (2001).
- Matsuda, T. *et al.* Oscillating rows of vortices in superconductors. *Science* **294**, 2136–2138 (2001).
- Grigorenko, A., Bending, S., Tamegai, T., Ooi, S. & Henini, M. A one-dimensional chain state of vortex matter. *Nature* **414**, 728–731 (2001).
- Vlasov, V. K. *et al.* Decoration of Josephson vortices by pancake vortices in  $\text{Bi}_2\text{Sr}_2\text{CaCu}_2\text{O}_{8-x}$ . *Phys. Rev. B* **66**, 014523 (2002).

29. Tokunaga, M. *et al.* Visualization of vortex chains in  $\text{Bi}_2\text{Sr}_2\text{CaCu}_2\text{O}_{8+\gamma}$  by magneto-optical imaging. *Phys. Rev. B* **66**, 060507(R) (2002).
30. Ooi, S. *et al.* Vortex matter transition in  $\text{Bi}_2\text{Sr}_2\text{CaCu}_2\text{O}_{8+\gamma}$  under tilted fields. *Phys. Rev. B* **63**, 20501(R) (2001).
31. Ooi, S. *et al.* Novel angular scaling of vortex phase transitions in  $\text{Bi}_2\text{Sr}_2\text{CaCu}_2\text{O}_{8+\gamma}$ . *Phys. Rev. Lett.* **82**, 4308–4311 (1999).
32. Mirković, J. *et al.* Stepwise behavior of vortex-lattice melting transition in tilted magnetic fields in single crystals of  $\text{Bi}_2\text{Sr}_2\text{CaCu}_2\text{O}_{8+\delta}$ . *Phys. Rev. Lett.* **86**, 886–889 (2001).
33. Savel'ev, S. & Nori, F. Experimentally realizable devices for controlling the motion of magnetic flux quanta in anisotropic superconductors. *Nature Mater.* **1**, 179–184 (2002).
34. Savel'ev, S., Marchesoni, F. & Nori, F. Manipulating small particles in mixtures far from equilibrium. *Phys. Rev. Lett.* **92**, 160602 (2004).
35. <<http://dml.riken.go.jp/vortex>>; <http://staff.bath.ac.uk/pyssb/1DMovies.htm>.
36. Bulaevskii, L. N., Ledvij, M. & Kogan, V. G. Vortices in layered superconductors with Josephson coupling. *Phys. Rev. B* **46**, 366–380 (1992).
37. Koshelev, A. E. Crossing lattices, vortex chains, and angular dependence of melting line in layered superconductors. *Phys. Rev. Lett.* **83**, 187–190 (1999).
38. Savel'ev, S. E., Mirković, J. & Kadowaki, K. London theory of the crossing vortex lattice in highly anisotropic layered superconductors. *Phys. Rev. B* **64**, 094521 (2001).
39. Perkins, G. J., Caplin, A. D. & Cohen, L. F. Dynamic interactions between pancake vortex stacks and Josephson vortices in  $\text{Bi}_2\text{Sr}_2\text{CaCu}_2\text{O}_{8+\delta}$  single crystals: relaxation and ratchets. *Supercond. Sci. Technol.* **18**, 1290–1293 (2005).
40. Motohira, N. *et al.* Single crystal growth of  $\text{Bi}_2\text{Sr}_2\text{Ca}_{a-1}\text{Cu}_b\text{O}_y$  superconductors by the floating zone method. *J. Ceram. Soc. Jpn* **97**, 1009–1014 (1989).
41. James, M. S., Stoddart, S. T. & Bending, S. J. Field penetration and surface barriers in superconducting  $\text{Bi}_2\text{Sr}_2\text{CaCu}_2\text{O}_{8+\delta}$  whiskers. *Phys. Rev. B* **56**, R5771–R5773 (1997).
42. Koshelev, A. E. Kink walls and critical behavior of magnetization near the lock-in transition in layered superconductors. *Phys. Rev. B* **48**, 1180–1191 (1993).
43. Avraham, N. *et al.* 'Inverse' melting of a vortex lattice. *Nature* **411**, 451–454 (2001).
44. Savel'ev, S. E. & Gorbachev, V. S. Microscopic model of critical state for the hard superconductor. *JETP* **83**, 570–581 (1996).

#### Acknowledgements

We gratefully acknowledge support from the EPSRC (UK) under grant No. GR/R46489/01, the ESF VORTEX network, the US NSA and ARDA under AFOSR contract No. F49620-02-1-0334, NSF grant No. EIA-0130383, and a Grant-in-Aid for Scientific Research from MEXT, Japan. Correspondence and requests for materials should be addressed to S.B.

#### Competing financial interests

The authors declare that they have no competing financial interests.

Reprints and permission information is available online at <http://npg.nature.com/reprintsandpermissions/>